Hydrodynamic stability of helical growth at low Reynolds number

Ariel Balter[1] and Jay X. Tang[2]
[1]*Department of Physics, Indiana University, Bloomington, Indiana 47405, USA*
[2]*Department of Physics, Brown University, Providence, Rhode Island 02912, USA*
(Received 11 December 2004; published 31 May 2005)

A cylindrical object growing at a low Reynolds number can spontaneously develop a helical shape. We have studied this phenomenon numerically, and our results may shed some light on the spontaneous formation of helical tails of a dense protein network observed in experiments on actin based motility. We also identify an unstable critical pitch angle which separates helices that straighten into rods from helices that flatten into planar curves as they grow. At the critical angle the pitch angle remains constant, whereas both helical diameter and pitch increase with the helical contour length.

DOI: 10.1103/PhysRevE.71.051912 PACS number(s): 87.16.−b, 87.10.+e, 87.15.−v

I. INTRODUCTION

Translating an irregularly-shaped object in a fluid at low Reynolds number will, in general, induce a concurrent rotation. The magnitude and axis of this rotation depend only on the shape of the object, the orientation of the object, and the translation vector (or velocity). Consider an object powered by a rigidly mounted engine, which produces constant thrust. In the body-centered reference frame, the thrust, or force, $\mathbf{f}$, is a constant vector. The velocity and angular velocity are also constant in this frame due to the drag tensor relationships $\mathbf{v}=A\mathbf{f}$ and $\boldsymbol{\omega}=B\mathbf{f}$ [1], where A and B depend only on the shape of the object.[1] In the observer frame we find that $\dot{\mathbf{v}}=\boldsymbol{\omega}\times\mathbf{v}$, $\dot{\mathbf{f}}=\boldsymbol{\omega}\times\mathbf{f}$, and $\dot{\boldsymbol{\omega}}=\boldsymbol{\omega}\times\boldsymbol{\omega}=0$. So the angular velocity vector is constant in the observer frame as well. As explained further in Appendix A, the geometry of the path can be determined from the rotation vector $\mathbf{k}(s)=\boldsymbol{\omega}(t)/|\mathbf{v}(t)|$ by associating it with the Darboux vector of the Frenet-Serret parametrization of the path. Constant $\mathbf{k}$ means the path is a straight line, circle or regular helix. Various microorganisms display these geometries in *helical klinotaxis* as they locate favorable environments [2].

In this paper we study a related issue. How would the hydrodynamic forces on an irregular object that is growing affect the growth? Inspired by a biological system, in which helical "tails" of densely gelled F-actin grow from N-WASP coated micron-sized beads immersed in a broth of appropriate proteins, we examine what would happen to an object that is pushed through a viscous fluid as it grows out from a fixed point in space in a constant direction. The growth process generates constant thrust, but in this case the shape of the object changes as the object grows. As hydrodynamic drag causes the object to rotate, new material is added at various angles. The surprising result from our simulations is that even with random perturbations, helical shapes naturally emerge.

Our specific goal is to examine the possible role of hydrodynamics in influencing the shape of "comet tails," or trails of a polarized network of actin filaments which form during the locomotion of many infectious pathogens such as listeria moncytogenes [3–5], rickettsia [5,6], and shigella [6,7], as well as subcellular organelles [8–12]. An enzyme coating on the surface of the bacteria (or other cargo) causes actin filaments to grow there preferentially, and this growth generates force via the energetically favorable addition of actin monomers to the tips of existing actin filaments in the gel. This process requires the intercalation of actin monomers at the bead surface. Viscous drag, possibly enhanced by interconnections with actin filaments in the surrounding solution, anchors the comet tail, and so the bacterium is pushed away from the existing tail.

Comet tail motility has been discussed extensively in the biological literature and is considered a prototype system for understanding the molecular mechanisms of cell locomotion. On one hand, this kind of motion appears in both deadly microbes and functional subcellular organelles. On the other hand, it provides a clear experimental arena in which to explore general features of cytoskeletal actin dynamics. This is because unlike other forms of actin based motility (e.g., filipodia and lamellipodia), which involve the complex dynamics of chemical signaling and control, the comet tail motility system is spontaneous, requiring only an enzyme coating on small object[2] and a few factors already present in a host cell cytoplasm. The raw material and energy come from the host cell, which plays only a passive role.

As a proof of this simplicity, comet tail motility can be completely reproduced in vitro. Micrometer-sized beads [13–15], liposomes [16] and oil drops [17], when coated with appropriate enzymes, have all been shown to initiate actin-based motility in tissue extracts and even artifical mixtures of essential proteins. This work was particularly inspired by some anomalous results of experiments in completely cell-free systems. Under certain conditions beads have been ob-

[1]This can also be thought of as decomposition of the viscous response into Stokeslets and rotlets. When the Reynolds number $\mathrm{Re}=0$, the response is a linear sum of these fundamental Green's function tensors.

[2]This property—that the motility relies almost entirely on constituents of the host cell—suggests it could also be possible to use this method for delivering drugs into cells.

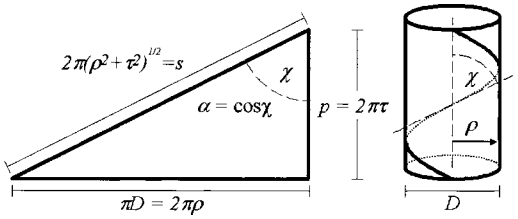

FIG. 1. Illustration of one turn of a helix "wrapped" and "unwrapped." As z increases along the vertical edge by one pitch, the distance along the helix increases by the hypotenuse, $s=p/\alpha$.

served to grow twin, symmetrical helical comet tails.[3] The observed mirror handedness of the tails places limits on the possible contribution of molecular handedness. Furthermore, the thickness of the tails is about the same as the bead diameter, and the scale parameters of the helices (Fig. 1) are just a few times this. So the helical tails represent a pattern emerging spontaneously at the largest length scales in the system. In this work, we explore the possibility that hydrodynamic forces play a role in this type of spontaneous pattern formation. Additionally, a separate recent study shows motile *listeria* that consistently follow right-handed helical trajectories [18]. Although the helicity of the actin filaments is thought to drive this pattern, the particular paths traced out are undoubtedly affected by hydrodynamic forces as well. Our model may provide an additional tool for analyzing these comet tails.

We turn now to the growth process. Out of the bead grows an object which is a thin, bent rod. Measurements of shape, structure and protein concentration on listerial comet tails, as well as manipulation of bead induced tails using laser tweezers suggest that they are rigid objects ($Y\sim10^3$–10^4 Pa) [19], and there is no indication of the bends in comet tails straightening out due to relaxation. On the other hand, there must still be some freedom for the tail to move relative to the bead where the tail grows since (1) the growth requires the intercalation of new material at the bead surface, and (2) the tails generally grow in curvy shapes. The general idea is of a rigid substance extruded into a fluid at low Reynolds number (Re) such that it has a degree of freedom to rotate at the point of generation. An analogy might be a stream of hot glue being injected into a cold bath of glycerin.

We have simulated this process and found that stable, helical growth naturally emerges, but with some irregular features. We looked at the growth dynamics for a range of helical seeds and sampled the statistics of helices which grow from random initial conditions. We also examined the effect of random perturbations to the growth. Although the system is simple to describe mathematically (Appendix A), it is analytically intractable to solve. Nevertheless, we try to explain the results within the theoretical context of the model in light of the simulation results.

[3]Private communications with Sebastian Wiesner and Marie-France Carlier, CNRS.

II. METHODS

Simulation

Our simulation runs as follows. We imagine a point on a plane from which material emerges normal to this plane in the form of thin cylindrical segments. We impose a translation of a fixed amount normal to the plane, calculate and perform the resulting rotation of the existing tail, and finally add the new piece of tail between the base of the existing tail (which now lies above the growth plane after translation and rotation) and the origin in the growth plane. There is no need to calculate the forces and torques since we can calculate the resulting rotation directly (6). We simplify our calculations by referring to a frame centered at the point of growth, where the assumed force due to growth is applied. In this frame the applied torque is identically 0. The resulting rotation does not depend on the viscosity of the fluid since the viscosity falls out of the rotation equation (explained later). Though seemingly paradoxical, this directly results from assuming the Reynolds number $\mathrm{Re}\ll1$. As a result, the only truly free parameter is the length of the growth segments (essentially the velocity at constant time steps), and to make the time steps effectively small we simply keep this length small compared to the size of the seed. In this sense, our simulation is "scale free." We choose the size of the seed helix, which is arbitrary, and we then pick the growth segment size to be small enough to get smooth growth.

We calculate the drag using the resistive force theory of hydrodynamics (RFT) [20] in which a curvy, slender object is modeled as a series of cylindrical elements which have drag coefficients per unit length both parallel and perpendicular to their symmetry axis such that $\mathbf{f}_\parallel=\zeta_\parallel\mathbf{v}_\parallel$ and $\mathbf{f}_\perp=\zeta_\perp\mathbf{v}_\perp$. Decomposing $\mathbf{v}$ into $\mathbf{v}_\parallel=\hat{\hat{\mathbf{l}}}\hat{\hat{\mathbf{l}}}\cdot\mathbf{v}$ and $\mathbf{v}_\perp=(\mathbf{1}-\hat{\hat{\mathbf{l}}}\hat{\hat{\mathbf{l}}})\cdot\mathbf{v}$, where $\hat{\mathbf{l}}$ is a unit vector pointing in the direction of an element of length l, we can write

$$\mathbf{f}=[\zeta_\parallel l\hat{\hat{\mathbf{l}}}\hat{\hat{\mathbf{l}}}+\zeta_\perp l(\mathbf{1}-\hat{\hat{\mathbf{l}}}\hat{\hat{\mathbf{l}}})]\cdot\mathbf{v}. \tag{1}$$

This implies a drag tensor

$$\mathbf{D}=l\zeta_\perp(\mathbf{1}-(1-q)\hat{\hat{\mathbf{l}}}\hat{\hat{\mathbf{l}}})=l\zeta_\perp(\delta_{i,j}-(1-q)\hat{l}_i\hat{l}_j). \tag{2}$$

The parameter $q=\zeta_\parallel/\zeta_\perp$ holds information about the relative importance of longitudinal and transverse drag. For a simple fluid, $q=1/2$. Long polymers can inhibit transverse motion of long objects, so a high concentration of long polymers will make q smaller. An object element at position $\mathbf{r}_n$ moves with a velocity $\mathbf{v}(\mathbf{r}_n)$ and experiences a force $\mathbf{f}(\mathbf{r}_n)=\mathbf{D}(\mathbf{r}_n)\mathbf{v}(\mathbf{r}_n)$, or more conveniently,

$$\mathbf{f}_n=\mathbf{D}_n\mathbf{v}_n. \tag{3}$$

The net force ($\mathbf{f}$) and torque ($\boldsymbol{\tau}$) on the object as a whole are linear functions of the velocity ($\mathbf{v}$) and angular velocity ($\boldsymbol{\omega}$) through the net drag tensors for the object as a whole. We calculate these tensors from the $\mathbf{D}_n$ via sums over all elements of the object using $\mathbf{f}_n=\mathbf{f}_{tot}+\boldsymbol{\omega}_{tot}\times\mathbf{r}_n$ and $\boldsymbol{\tau}_n=\mathbf{r}_n\times\mathbf{f}_n$:

$$\begin{pmatrix} \mathbf{f}_{drag} \\ \boldsymbol{\tau}_{drag} \end{pmatrix} = \begin{pmatrix} \sum_n \mathbf{f}_n \\ \sum_n \boldsymbol{\tau}_n \end{pmatrix} = \begin{bmatrix} \sum_n \mathbf{D}_n & \sum_n \mathbf{D}_n \times \mathbf{r}_n \\ \sum_n \mathbf{r}_n \times \mathbf{D}_n & \sum_n \mathbf{r}_n \times \mathbf{D}_n \times \mathbf{r}_n \end{bmatrix} \begin{pmatrix} \mathbf{v} \\ \boldsymbol{\omega} \end{pmatrix} = \begin{bmatrix} \mathbf{D}_{LL} & \mathbf{D}_{LR} \\ \mathbf{D}_{RL} & \mathbf{D}_{RR} \end{bmatrix} \begin{pmatrix} \mathbf{v} \\ \boldsymbol{\omega} \end{pmatrix}. \quad (4)$$

To generate translation, a force must be applied at the base of the tail, which lies at the origin in the growth plane, $\mathbf{r}_0$. We refer torque calculations to this point. Force balance with perfect drag dictates that

$$\begin{pmatrix} \mathbf{f}_{tot} \\ \boldsymbol{\tau}_{tot} \end{pmatrix} = \begin{pmatrix} \mathbf{f}_{applied} \\ \boldsymbol{\tau}_{applied} \end{pmatrix} + \begin{pmatrix} \mathbf{f}_{drag} \\ \boldsymbol{\tau}_{drag} \end{pmatrix} = \begin{pmatrix} 0 \\ 0 \end{pmatrix}. \quad (5)$$

Since we choose $\mathbf{r}_0$ such that $\boldsymbol{\tau}_{applied}=\mathbf{r}_0\times\mathbf{f}_{applied}=0$ we automatically impose the additional constraint that $\boldsymbol{\tau}_{drag}=0$. By doing so, we can write

$$\boldsymbol{\omega} = -\mathbf{D}_{RR}{}^{-1}\mathbf{D}_{RL}\mathbf{v}. \quad (6)$$

At time t, we describe the tail or object by an ordered set of points which represent the meeting points (or nodes) between hypothetical, small, cylindrical elements. Let us denote this set of points, which form the "tail," by an $N\times 3$ matrix (or "hypervector")

$$\mathbf{T}(t) = \begin{bmatrix} \mathbf{r}_0 \\ \mathbf{r}_1 \\ \mathbf{r}_2 \\ \vdots \\ \mathbf{r}_N \end{bmatrix} = \begin{bmatrix} 0 & 0 & 0 \\ x_1 & y_1 & z_1 \\ x_2 & y_2 & z_2 \\ \vdots & \vdots & \vdots \\ x_N & y_N & z_N \end{bmatrix}. \quad (7)$$

To evolve $\mathbf{T}$, we calculate $\mathbf{v}$ and $\boldsymbol{\omega}$ by (6) and construct the rotation operator $\mathbf{R}(t)\equiv R_{lm}(t)=\exp[-\Delta t\omega_k(t)\varepsilon_{klm}]$. We use another hypervector,

$$\mathbf{V}(\mathbf{t}) = \begin{bmatrix} \mathbf{v}_0 \\ \mathbf{v}_0 \\ \vdots \\ \mathbf{v}_0 \end{bmatrix} \quad (8)$$

to translate every element of the tail. Note that in our simulation, $\mathbf{v}_0$ represents each added segment, and has units of length (the time is implicitly one step). To update our object, we first rotate and then translate the existing tail

$$\mathbf{T}(t+\Delta t) = \mathbf{T}(t)\mathbf{R}(t)^T + \mathbf{V}(t). \quad (9)$$

The base of the tail is no longer at the origin after this translation, so we finally lengthen the tail by adding a new node at the origin. There are now $N+1$ points. Each $\mathbf{r}_n$ is relabled $\mathbf{r}_{n+1}$ and we create a new $\mathbf{r}_0=(0\ 0\ 0)$,

$$\mathbf{T} \rightarrow \begin{bmatrix} (0\ 0\ 0) \\ \mathbf{T} \end{bmatrix}. \quad (10)$$

In some simulations we also included random perturbations to the growth. We perturbed the growth by choosing a random orientation for $\mathbf{v}_0$. While unperturbed sections point in the $\hat{\mathbf{z}}$ direction, and the perturbed sections point toward

$$\cos\phi\sin\theta\,\hat{\mathbf{x}} + \sin\phi\sin\theta\,\hat{\mathbf{y}} + \cos\theta\,\hat{\mathbf{z}}, \quad (11)$$

where ϕ is a uniformly distributed arbitrary number $[0,2\pi]$ and θ a random number with the mean value 0 and variance σ^2. We found that these perturbations do not greatly affect the stability of growth.

We now address the role of viscosity. A proportionality factor between $\boldsymbol{\omega}$ and $\mathbf{v}$ can only have units of l^{-1}. The units of $\mathbf{D}_{RR}$ and $\mathbf{D}_{RL}$ are $l^3\zeta$ and $l^2\zeta$, respectively, so the combination $-\mathbf{D}_{RR}{}^{-1}\mathbf{D}_{RL}$ [see Eq. (6)] does have the expected units—the viscosity divides out. This does not mean that viscosity is not important for this system—it is crucial. In fact, our entire theory, including the definition of drag tensors, is based on the $\mathrm{Re}\rightarrow 0$ limit. That ζ falls out merely tells us that in this limit, the *particular* value of the viscosity does not affect the hydrodynamic response of the tail in terms of its net rotation.

III. ANALYSIS OF HELIX GEOMETRY

Two convenient parameters for describing the shape (or instantaneous shape) of a helix are the pitch p (distance between turns) and the diameter D (Fig. 1). One intuitive way to make a helix would be to feed a pipe cleaner through one's fingers at a constant rate, while simultaneously (or alternately) bending it and twisting it. For each time step:

(1) Push the pipe cleaner a little further through one's fingers and thumb.

(2) Apply a small twist with one's fingers and thumb.

(3) Take the other hand and bend over a small angle at the base of the exposed part.

If one bends and twists at constant rates one gets a regular helix. Steadily slowing the rates of bending or twisting yields a helix that becomes wider and steeper. The two control parameters are the "bend" and "twist." Since the twist vector runs parallel to the wire, we call it $\mathbf{k}_\parallel$ and the bend vector $\mathbf{k}_\perp$. These vectors are rotation rates with respect to distance. The following relations hold (Appendix A):

$$p = 2\pi|\mathbf{v}|\frac{|\boldsymbol{\omega}_\parallel|}{|\boldsymbol{\omega}|^2} = 2\pi\frac{|\mathbf{k}_\parallel|}{|\mathbf{k}|^2}, \quad D = 2|\mathbf{v}|\frac{|\boldsymbol{\omega}_\perp|}{|\boldsymbol{\omega}|^2} = 2\frac{|\mathbf{k}_\perp|}{|\mathbf{k}|^2}, \quad (12)$$

where $\mathbf{v}$ is the feeding rate. The ratio of bend and twist determines the "shape" of the helix, or how it looks. This ratio is related to the "pitch angle," χ, by

$$\tan\chi = \frac{|\mathbf{k}_\perp|}{|\mathbf{k}_\parallel|} = \frac{\pi D}{p}. \quad (13)$$

The relations between these parameters are illustrated in Fig. 1 and are detailed in Appendix A.

IV. RESULTS

Our most important result is that the growth of a generalized, expanding helix can emerge spontaneously even when we run simulations from random initial conditions [Fig. 2(a)]. The pitch and diameter increase proportionally, but the axis and the helical angle remain constant. We used Eq. (11) to build the first three segments and then let the

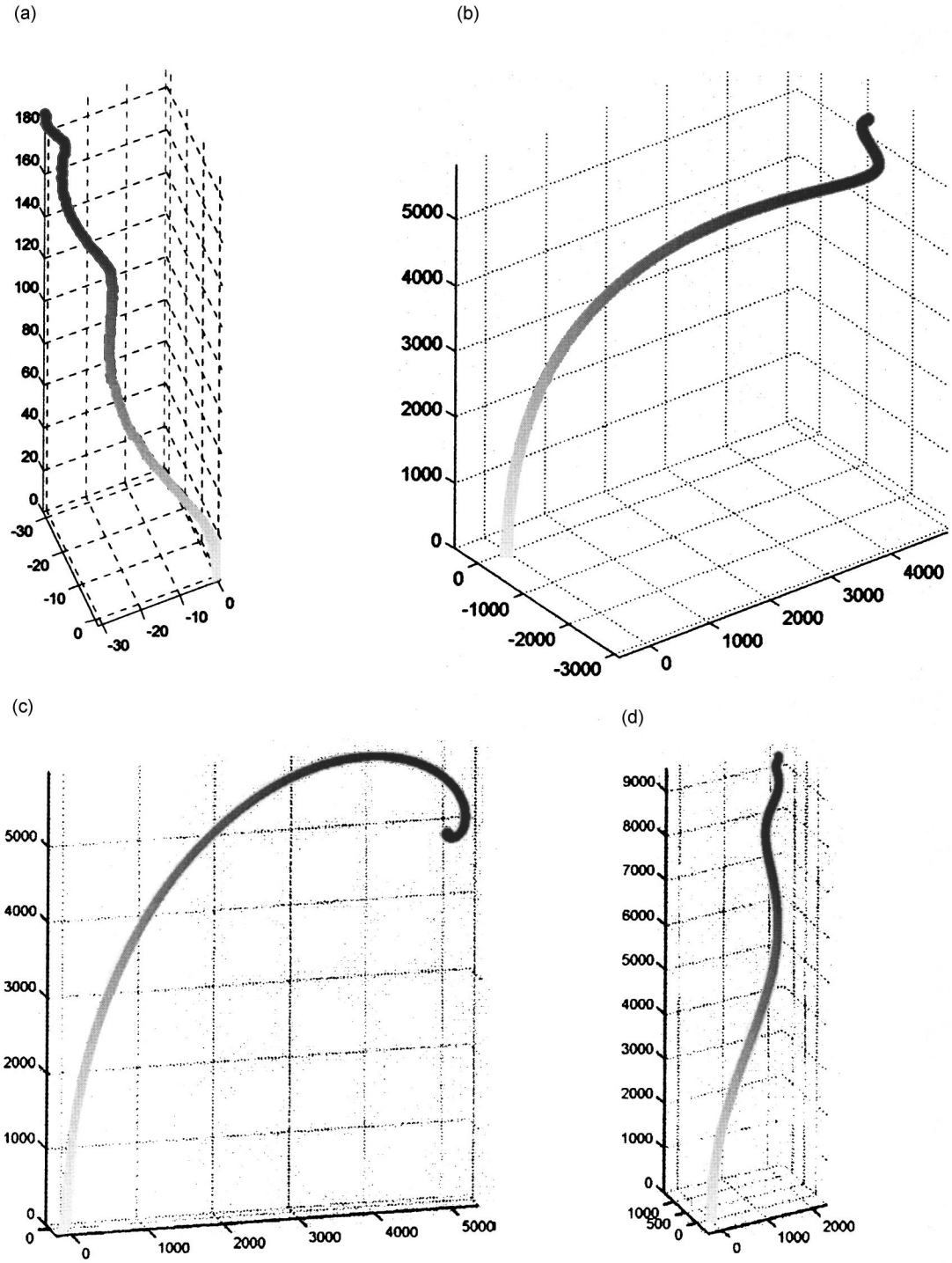

FIG. 2. Representative simulation results showing helices, which grow out of a range of seeds. (a) The result of a single simulation run for a helix growing out of the *x*-*y* plane. The "older" units are shaded darker. This helix was grown for 200 additional units from a random seed three units long. (b) A helix grown at $\chi=\chi_{crit}$ for 10 000 steps from a seed helix 300 steps long. (c) A helix grown for 10 000 steps from a seed with a large pitch angle ($\chi=70°$) 300 steps long. (d) A helix grown for 10 000 steps from a seed with a small pitch angle ($\chi=20°$) 300 steps long.

simulation run. Even random perturbations to the subsequent growth did not alter this result.

Understandably, as the tail gets longer, a perturbation to a single segment becomes less and less important. An important additional insight gained from these tests is how the initial "seed" determines the shape of the emerging helix. Essentially, the three initial segments form a minimum structure needed to define an initial bend and twist. To show this we sampled the statistics of the helical parameters of randomly generated helices. Referring back to (11), $\Delta\phi$, the difference of successive azimuthal angles, is essentially a "twist" and $\Delta\theta$ a "bend," i.e., $|\mathbf{k}_{\|}|=|\Delta\phi|$ and $|\mathbf{k}_{\perp}|=|\Delta\theta|$. Ac-

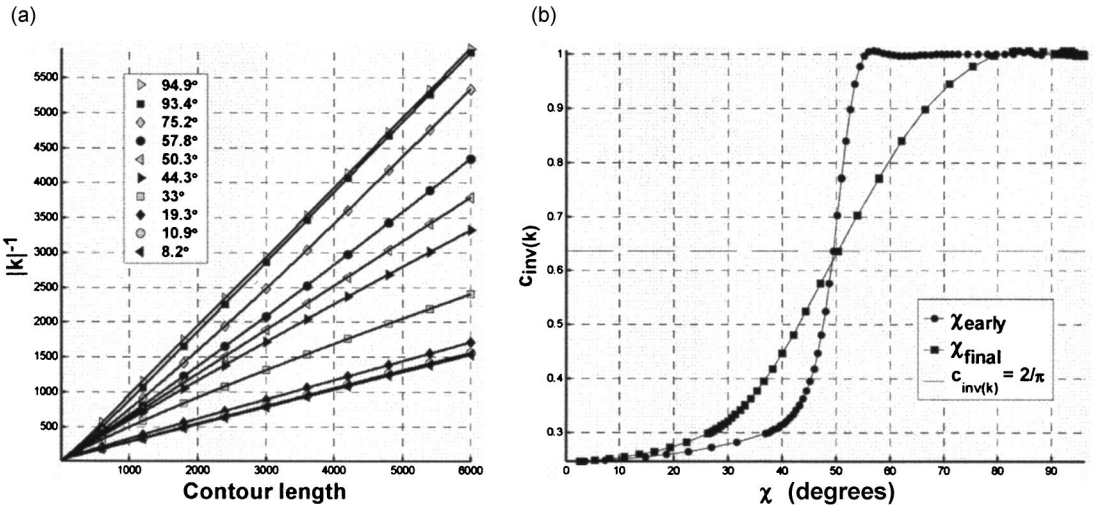

FIG. 3. Simulation results showing progression of helical shapes depending on the initial and early stage helical angles. (a) The inverse of the magnitude of the rotation vector, $|\mathbf{k}|^{-1}$, increases linearly with length as the helix grows. This result agrees with the theory. (b) The slope, c, of the line $|\mathbf{k}|^{-1}=cl$ for various values of χ shows a transition at χ_{crit}, where $c_{inv(k)}=2/\pi$. χ_{early} is the value of χ after it has stabilized in about 150 time steps.

cording to (13), $\tan\chi=|\mathbf{k}_\perp|/|\mathbf{k}_\parallel|=|d\theta/ds|/|d\phi/ds|$ (in an instantaneous sense). To approximate the result of randomly chosen θ and ϕ we look at[4]

$$\tan\chi \cong \frac{\langle|\Delta\phi|\rangle}{\pi\langle|\Delta\theta|\rangle} = \frac{\pi^{1/2}}{3\sigma} = \frac{0.591\ldots}{\sigma}.$$

We do find this functional dependence on σ in our simulations where we get

$$\left\langle \frac{|\phi|}{|\theta|} \right\rangle \approx \frac{0.7\pm0.1}{\sigma}.$$

To better understand the stability we ran long-time simulations with fixed helical seeds representing a range of initial pitch angles. We used seed helices with $\chi=n\pi/48$ for $n\in\{1\ldots23\}$, giving p/D a range of values $\sim$0.07, 0.14,…, and 15.26. For each pitch angle and in each of 100 trials, we let the growth continue for 6000 time steps, generating 2–6 full turns of a helix. The typical results are illustrated in Figs. 2(b)–2(d) for 10 000 time steps. When the initial conditions are a regular helix, the tail grows into an expanding helix that is heavily influenced by the seed helix. One interesting effect is that even for very large seeds (4–5 turns) the first growth step does not match the seed helix, a property explored in detail later. This is evidently another manifestation of the fact that regular helical growth is not stable. Instead, the stable growth is a generalized helix with expanding pitch and diameter.

[4]The true statistic average $\langle|\Delta\phi|/|\Delta\theta|\rangle$ is divergent. Perturbations in the subsequent simulation ultimately drive the system away from the $\Delta\theta=0$ case, but corrections to the approximate statistics would involve subsequent hydrodynamic interactions.

V. SCALING AND CRITICAL ANGLES

Referring back to (6), $\mathbf{D}_{RR}{}^{-1}\mathbf{D}_{RL}$ scales like s^{-1}, where s is the contour length of the tail, so we expect

$$|\mathbf{k}(s)|^{-1} = \frac{\sqrt{p(s)^2+[\pi D(s)]^2}}{2\pi} \approx cs \tag{14}$$

for some constant, c (recall that $|\mathbf{v}|$ is held constant). This linear relationship for $|\mathbf{k}|$ does emerge in our simulations [Fig. 3(a)]. However, the individual components $|\mathbf{k}_\parallel|=\tau|\mathbf{k}|=(p/2\pi)|\mathbf{k}|$ and $|\mathbf{k}_\perp|=\rho|\mathbf{k}|=(D/2)|\mathbf{k}|$ do not consistently scale linearly [see, for instance, Fig. 4(a)].

Interestingly, we also notice a critical angle that determines the scaling properties of $|\mathbf{k}|$, P and D, and other parameters as well. The diameter evolves close to linear and makes a transition at χ_{crit} where the coefficient $c_{diameter}$ goes from >1 to <1 [Fig. 4(c)]. The pitch grows almost linearly for angles above critical angle $50.3°<\chi_{crit}<53.8°$, but a close inspection shows that it is actually only linear at χ_{crit} (Fig. 4). A magnified display around the critical range shows that χ_{crit} represents a maximum for c_{pitch} and an inflection point for $c_{diameter}$ [Fig. 4(d)].

When we examine the value of the slope, $c_{inv(k)}$ in the expression of $|\mathbf{k}|^{-1}$ as in Eq. (14), we see two regimes and the crossover appears to be at χ_{crit} [Fig. 3(b)], where the slope happens to be $2/\pi$. A similar transition appears in the graph of the final (evolved) value of χ versus early but stabilized values [Fig. 5(b)]. Here the transition at $\chi_{final}=\chi_{crit}$ goes from a linear regime to what appears to be a stable oscillatory point at $\chi_{final}=90°$. The critical angle shows up again in the evolution of the value of χ, the pitch angle [Fig. 5(a)]. As stated before, the value of χ is generally not constant as the helix grows. It makes a transition from increasing when $\chi<\chi_{crit}$ to decreasing when $\chi>\chi_{crit}$. χ_{crit} appears to be a stable value at which the helix grows in a special way: the pitch and diameter each increase but always in a way that

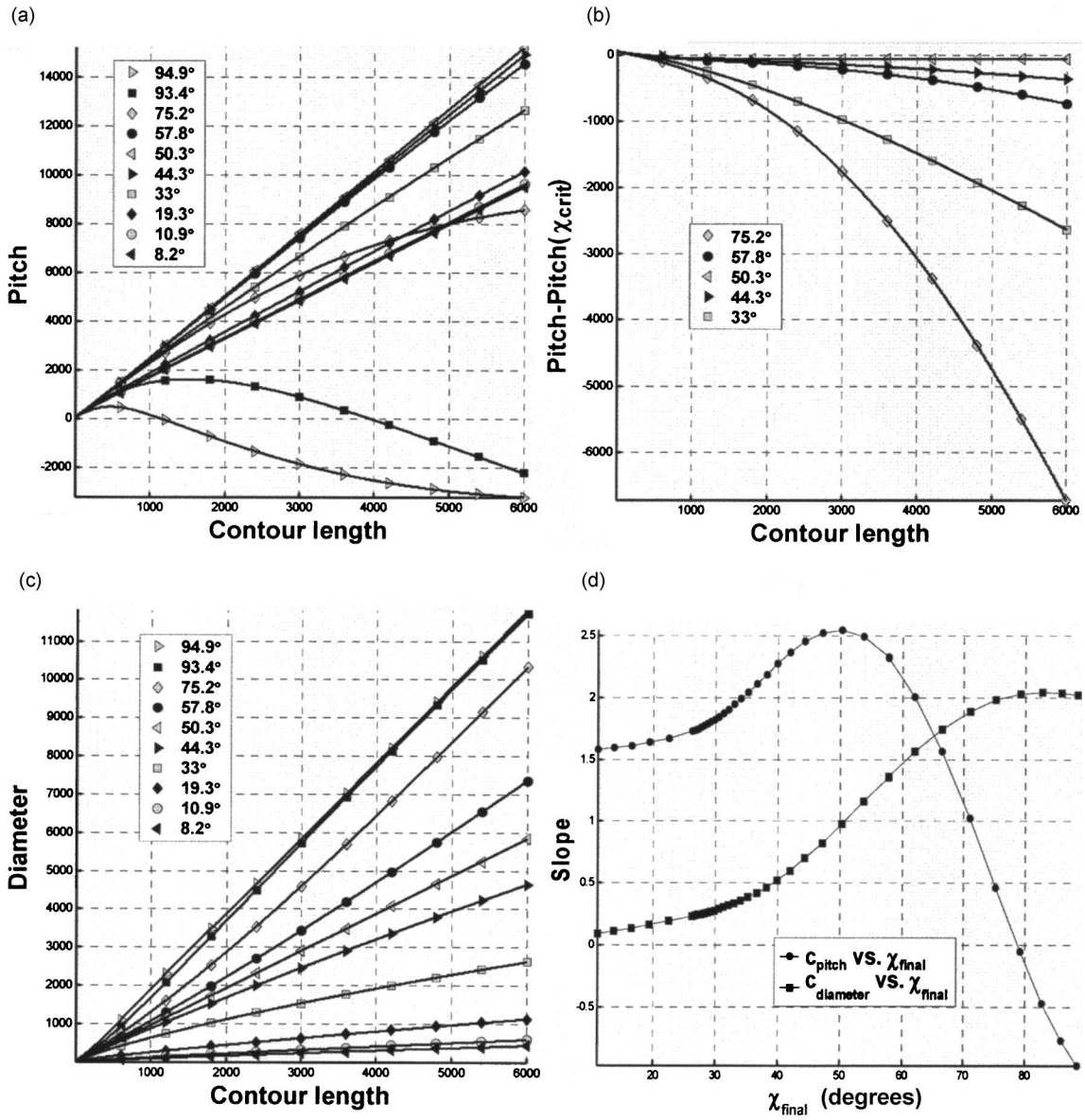

FIG. 4. Evolution of helical pitch and diameter above and below the critical pitch angle. (a) The pitch shows a transition from a regime of nonlinear growth at high pitch angle to linear growth at below χ_{crit}. (b) In order to illustrate the transition at the critical pitch angle χ_{crit}, deviation is plotted for the lines for χ near χ_{crit} from the line for χ_{crit}, $pitch(\chi)-pitch(\chi_{crit})$. (c) $c_{diameter}$ for various values of χ shows a transition from $c<1$ to $c>1$ at χ_{crit}. (d) To further illustrate that the slope is greatest at χ_{crit}, the slopes of pitch and diameter are plotted as functions of χ. The diameter exhibits a fairly linear increase with the contour length l. For the pitch, we calculate c_{pitch} for only the slope of the last 10% of the curve.

preserves the pitch angle. We have no explanation for the origin of the critical values. But we find it interesting that χ_{crit} appears close to the observed value of χ in the twin tails observed experimentally [21]. However, this cannot explain the phenomenon since χ_{crit} appears to be an unstable critical point, i.e., sample runs that start out away from χ_{crit} do not converge to χ_{crit} (Fig. 5).

VI. CONCLUSION

These simulations show that a regular pattern of growth can emerge when an object in a low Reynolds number environment grows in such a way that the bulk of the object pushes away from where the growth takes place. The object may spontaneously grow into an expanding helix in which the pitch and diameter increase as the growth continues. We identify a critical angle at which the growth stabilizes such that the pitch angle remains constant (although the pitch and diameter still individually increase).

This study has been inspired by a biomimetic system in which an enzyme coated bead grows a pair of symmetric helical "comet tails." We report without explanation that the critical angle mentioned above is very close to the observed pitch angle in these helical growths. But the actual role hydrodynamics might play in the formation of twin helical comet tails remains unclear, especially since χ_{crit} is not a

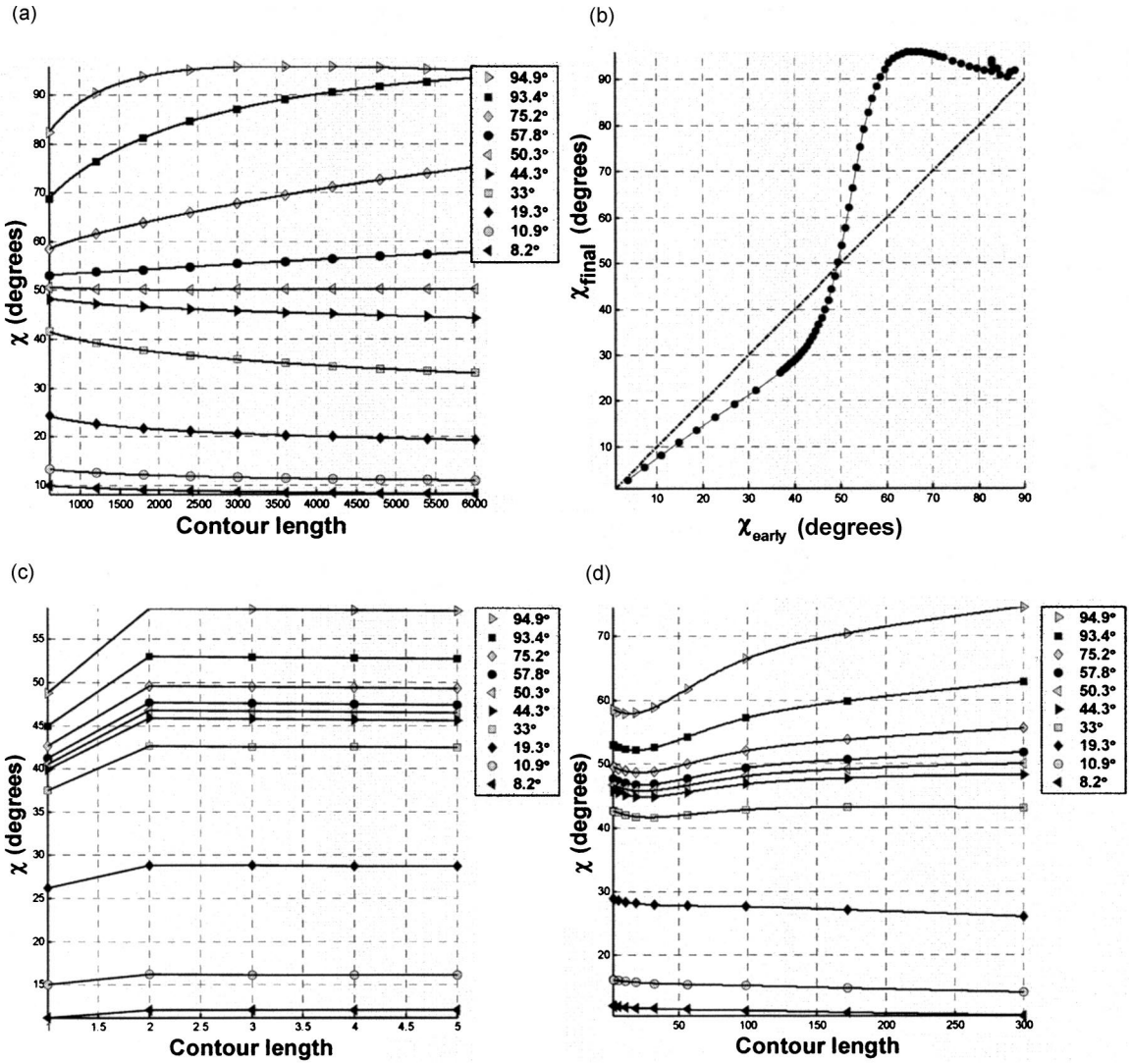

FIG. 5. Simulation results relating helical angles of an initial seed, the early progression, and the stabilized shape. (a) The only value of χ for which χ remains constant is χ_{crit}. Either above or below this value, the pitch angle diverges from χ_{crit}. (b) The ultimate value of χ during growth is a function of χ_{seed}, the pitch angle of the seed helix. Notice that for $\chi<\chi_{crit}$ points lie below the dotted line showing $\chi_{final}=\chi_{initial}$, and above the line for $\chi>\chi_{crit}$. Thus χ diverges away from χ_{crit} during growth. Note that the dotted line does not cross the graph at χ_{crit} as it should if χ_{crit} really represents the value for which $d\chi/ds=0$. The reason is that the seed helix is a regular helix, and therefore does not represent stable growth. That is the origin of the counterintuitive result that, for a regular helix seed to end up with $\chi=\chi_{crit}$, the original value of χ is not χ_{crit}. To get around this, we look at the "stabilized" value of χ after the initial jump. We could avoid this by using a seed helix with the growth pattern that spontaneously emerges, but this is difficult to do in practice. (c) The initial jump in χ is most noticeable for addition of the first segment. (d) The value of χ stabilizes after about 200 time steps out of 6000.

stable critical point. Clearly in the case of the comet tails there is much more going on. For instance, the pitch and diameter remain more or less constant in the growth of helical comet tails.

In summary, we have identified a form of spontaneous pattern formation due to hydrodynamic forces. The role of hydrodynamics has been examined in this work as one possible contribution to the overall dynamics of helical comet tails. More study may reveal the full picture for the comet tail system and lead to a better overall understanding of cytoskeletal actin dynamics. Whether or not the mechanism analyzed in this work is relevant to other physical systems, and perhaps even manufacturing processes, remains to be seen.

APPENDIX A: MATHEMATICAL DESCRIPTION OF A HELIX

A helix trajectory is formed as one constantly turns left (or right) while climbing uphill. The path ones travels can be fully described by two parameters: the turning radius (how sharply one turns left or right) and the pitch (how steeply uphill one climbs). The first parameter, ρ, is the radius of the circle you make when viewed from directly above, and the second can take the form of an angle, χ (the pitch angle to the vertical) or a wavelength, p, the wavelength of the sine wave you make as viewed directly from the side. A simple mathematical description of this is $\vec{\mathbf{r}}=\rho\cos(2\pi/p)z\hat{\mathbf{x}}+\rho\sin(2\pi/p)z\hat{\mathbf{y}}+z\hat{\mathbf{z}}$, but if the axis of the helix is in a gen-

eral direction, say $\hat{\mathbf{e}}_3$, then we must describe this helix by $\vec{\mathbf{r}} = \rho\cos(2\pi z/p)\hat{\mathbf{e}}_1 + \rho\sin(2\pi z/p)\hat{\mathbf{e}}_2 + z\hat{\mathbf{e}}_3$. If we use the distance, s, along the helix as the parameter instead of the height, z, we can write

$$\vec{\mathbf{r}} = \rho\cos\frac{\alpha s}{\tau}\hat{\mathbf{e}}_1 + \rho\sin\frac{\alpha s}{\tau}\hat{\mathbf{e}}_2 + \alpha s\hat{\mathbf{e}}_3, \tag{A1}$$

where $\tau = p/2\pi$,[6] and $\alpha = \tau/\sqrt{\tau^2+p^2} = \cos(\chi)$ (Fig. 1). χ is the constant angle a helix makes with its axis, by which we mean the angle between the axis and the tangent vector $\hat{\mathbf{t}} = d\vec{\mathbf{r}}/ds$. If the axis of the helix is a vector $\hat{\mathbf{k}}$, then $\cos\chi = \hat{\mathbf{t}}\cdot\hat{\mathbf{k}} = \alpha$. Another way to derive (A1) as the representation of a helical space curve is to model the curve obtained if we wrap $\hat{\mathbf{t}}$ around the rotation vector $\mathbf{k}(s)$ which points along the axis of the helix and a tangent vector to the helix at some point s_0, $\hat{\mathbf{t}}(s_0)$. If the helix is uniform, $\mathbf{k}(s) = \mathbf{k}$. The tangent vector along the helix at a distance s from s_0 is

$$\hat{\mathbf{t}}(s) = \exp[(s-s_0)\mathbf{k}]\times\hat{\mathbf{t}}(s_0) = \exp[-(s-s_0)k_i\varepsilon_{ijk}]\hat{t}_{jk}(s_0) \tag{A2}$$

so $\cos\chi = \mathbf{k}\cdot\hat{\mathbf{t}}(s) = \mathbf{k}\cdot\hat{\mathbf{t}}(s_0)$ and the space curve of the helix is $\mathbf{r} = \int_{s_0}^{s}\hat{\mathbf{t}}(s')ds'$. In the Frenet-Serret representation, $\vec{\mathbf{k}}$ is equivalent to the "Darboux vector."

[6]Not to be confused with the torque vector $\boldsymbol{\tau}$.

Comparing (A1) and (A2) (when fully evaluated) leads to the relations

$$\rho/\tau = \pi D/P = |\mathbf{k}_\perp|/|\mathbf{k}_\parallel|,$$

$$\rho = |\mathbf{k}_\parallel|/k^2,$$

$$\tau = |\mathbf{k}_\perp|/k^2, \tag{A3}$$

with $\mathbf{k}_\parallel = \hat{\mathbf{t}}(\mathbf{k}\cdot\hat{\mathbf{t}})$, and $\mathbf{k}_\perp = \mathbf{k} - \hat{\mathbf{t}}(\mathbf{k}\cdot\hat{\mathbf{t}}) = (\mathbf{1} - \hat{\mathbf{t}}\hat{\mathbf{t}})\mathbf{k}$.

Allowing s to increase is equivalent to the helix growing by material being added to one end. Double helical tails grow in a more peculiar way: the growth occurs at a fixed point in space (at the bead surface) and the tails rotate and translate to accommodate the new growth. But the mathematical description is almost the same. For a dynamic description of a growing helix we replace $\mathbf{k}(s)$ by $\boldsymbol{\omega}(t) = |\mathbf{v}(t)|\mathbf{k}(s)$ where $|\mathbf{v}(t)| = ds/dt$ is the growth rate of the helix. The point s now represents the material added at time $t = (s - s_0)/|\mathbf{v}|$. Geometrically, the helix "wraps" around $\mathbf{k}$, so $|\mathbf{k}(t)|$ tells how many turns are forming as a function of linear distance (tail growth), and $|\boldsymbol{\omega}(t)|$ as a function of time. Since $|\mathbf{k}(t)|$ governs the geometry of the helix, it can be measured from a single still picture, while $|\boldsymbol{\omega}(t)|$ also includes information about the instantaneous growth rate.

[1] L. D. Landau and E. M. Lifshitz, *Fluid Mechanics*, 2nd ed., Course of Theoretical Physics Vol. 6 (Butterworth-Heinemann, Oxford, 1998), p. 539.
[2] H. C. Crenshaw, Bull. Math. Biol. **55**, 197 (1993).
[3] L. G. Tilney and D. A. Portnoy, J. Cell Biol. **109**, 1597 (1989).
[4] L. A. Cameron, *et al.*, Nat. Rev. Mol. Cell Biol. **1**, 110 (2000).
[5] E. Gouin, M. D. Welch, and P. Cossart, Curr. Opin. Microbiol. **8**, 35 (2005).
[6] R. A. Heinzen, *et al.*, Infect. Immun. **67**, 4201 (1999).
[7] T. P. Loisel, *et al.*, Nature (London) **401**, 613 (1999).
[8] F. Zhang, F. S. Southwick, and D. L. Purich, Cell Motil. Cytoskeleton **53**, 81 (2002).
[9] J. Taunton, *et al.*, J. Cell Biol. **148**, 519 (2000).
[10] C. Bazinet and J. E. Rollins, Evol. Dev. **5**, 379 (2003).
[11] M. P. Stevens and E. E. Galyov, Int. J. Med. Microbiol. **293**, 549 (2004).
[12] K. Breitbach, *et al.*, Cell. Microbiol. **5**, 385 (2003).
[13] L. A. Cameron, *et al.*, Mol. Biol. Cell **15**, 2312 (2004).
[14] L. A. Cameron, *et al.*, Proc. Natl. Acad. Sci. U.S.A. **96**, 4908 (1999).
[15] S. Wiesner, *et al.*, J. Cell Biol. **160**, 387 (2003).
[16] A. Upadhyaya and A. van Oudenaarden, Curr. Biol. **13**, R734 (2003).
[17] H. Boukellal, *et al.*, Phys. Rev. E **69**, 061906 (2004).
[18] W. L. Zeile, *et al.*, Cell Motil. Cytoskeleton **60**, 121 (2003).
[19] F. Gerbal, *et al.*, Eur. Biophys. J. **29**, 134 (2000).
[20] R. E. Johnson and C. J. Brokaw, Biophys. J. **25**, 113 (1979).
[21] S. Wiesner, M.-F. Carlier, D. Pantaloni, A. Balter, and J. X. Tang (unpublished).